



OPEN

Environment impact and probabilistic health risks of PAHs in dusts surrounding an iron and steel enterprise

Xiaofeng Wei¹, Chun Ding^{1,2}, Chunzhu Chen¹, Li Zhu¹, Guiqin Zhang¹ & Youmin Sun¹✉

Dust can be regarded as environmental medium that indicates the level and spatial distribution of polycyclic aromatic hydrocarbons (PAHs) coming from different pollution sources. In this study, samples including road dust, roof dust, and bare soil near an iron and steel enterprise (ISE) in Laiwu city of North China were collected. To assess the environment impact, atmosphere particulates and one flue dust from a coking plant were simultaneously sampled. Sixteen USEPA PAHs were detected quantitatively by Gas Chromatography Mass Spectrometry (GC-MS). A laser particle size analyzer was used to obtain the grain size of the dust particle samples. The results showed that PAH concentrations displayed great variability in the dust samples. The Σ_{16} PAHs concentration was found to be between 0.460 and 46.970 $\mu\text{g/g}$ (avg \pm sd 10.892 \pm 1.185 $\mu\text{g/g}$) in road dust, between 0.670 and 17.140 $\mu\text{g/g}$ (avg \pm sd 6.751 \pm 0.692 $\mu\text{g/g}$) in roof dust, and 13.990 \pm 1.203 $\mu\text{g/g}$ in bare soil. In the environment atmosphere sites, the Σ_{16} PAHs value in $\text{PM}_{2.5}$ constituted a very large proportion of PM_{10} , indicating that PAHs in finer particle sizes should be given greater emphasis. The Σ_{16} PAHs concentration was relatively high in the area close to the ISE because of the great impact of the ISE industrial activities. PAH concentration curves were similar, and the most abundant individual PAHs in the atmosphere sites were BbF, BkF, and Flu, and BbF, BkF, and Chry in dusts. Toxicity analysis revealed that PAHs with four rings, including carcinogenic PAHs, were the dominant pollutants in the studied area. The toxic equivalency value (TEQ_{Bap}), the carcinogenic health risk assessment value recommended by the US EPA, was calculated for seven carcinogenic PAHs, revealing that they account for more than 93.0% of the total TEQ_{Bap} of the 16 PAHs and indicating the major toxic equivalent concentration contributor. Incremental lifetime cancer risk (ILCR) estimation results showed that PAHs tended to bring about great health risks through skin contact, followed by ingestion and inhalation. By comparison, road dust exhibited greater carcinogenic risks than roof dust, and bare soil may undergo heavier pollution. Therefore, the results of this study would be helpful in the effort to understand the PAHs pollution from the steel industry, which will provide some guidance for the probabilistic assessment of local health risks.

Polycyclic aromatic hydrocarbons (PAHs), a class of persistent semi-volatile organic pollutants with characteristics of high toxicity and strong metamorphism, are one of the first discovered environmental carcinogens¹⁻³. PAHs consist of over 200 organic compounds, of which 16 are included in the list of priority controlled pollutants by the United States Environmental Protection Agency⁴. Numerous studies have revealed the main sources of PAHs to be residential coal burning, garbage incineration, activation of internal combustion engines, and various industrial activities such as coke production, oil refining, aluminum production, and smelting of non-ferrous metals⁵. It is reported that PAH pollution in industrial areas is more serious than that in residential areas; thus, many studies have reported PAH concentrations in the areas surrounding coal storage, coking and power plants, and iron and steel enterprises (ISE)⁶⁻⁸. Notably, the ISE performs multiple production steps and long-milling techniques, such as sintering, coking, iron smelting, and steelmaking, and each step contains several combined processes that lead to PAH pollution⁹.

¹School of Municipal and Environmental Engineering, Shandong Jianzhu University, Jinan 250101, Shandong, China. ²Clear Science and Technology Company Limited, Jinan 100029, Beijing, China. ✉email: ymsun@sdjzu.edu.cn

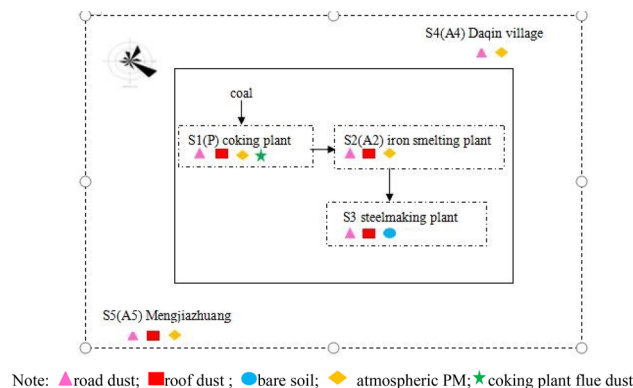


Figure 1. Spatial distribution of the sampling sites.

With improvements in technology, particles and PAHs from tail pipe emissions have been significantly reduced. However, atmospheric PAHs, which escape photo-degradation in the air and treatment from the tail gas equipment can accumulate in environmental media through dry and wet deposition¹⁰. Moreover, with the expansion of industrialization and urbanization in China, PAH emissions have maintained an increasing trend, which means that the impact of PAHs on society has gradually increased¹¹. It is reported that PAH levels have clear temporal and spatial distribution characteristics in China: PAH concentrations in winter are significantly higher than in other seasons^{12,13}, and in northern cities, they are higher than in southern cities¹⁴. Researchers have given attention to the characteristics, concentrations, and sources of PAHs in different environmental media^{15,16}. In most of these studies, the status of PAH pollution has been evaluated in the surrounding soil, street dust, water, atmosphere, and other environmental media or biological systems^{17–20}, whereas research on PAHs in different types of dust is quite limited. In addition, it is very important to study the influence of PAHs on the surrounding environment in air-dust media.

Laiwu lies in the middle of Shandong Province that the third largest economic province in northern China and has iron and steel production plants. It has an annual production capacity of 3 million tons of fine metal plates, sheets, and strips and 600,000 tons of stainless steel. In the present study, road dust, roof dust, bare soil, and atmosphere particles were collected from the ISE. The concentration level and environmental impact of 16 PAHs in dusts surrounding the ISE were assessed. Also, incremental lifetime carcinogenic risk due to exposure to PAHs in dust was evaluated. These findings can serve as a scientific basis for the control of PAH pollution in the areas surrounding the ISE.

Materials and methods

Sample sites and collection. According to the main producing process of ISE, dominant wind direction of the region and the surrounding villages, five sample sites surrounding an ISE were selected based on their representativeness of the area in Laiwu City. The detailed information for the sampling sites are as follows: site 1 (S1): coking plant, site 2 (S2): iron smelting plant (including sintering), site 3 (S3): steelmaking plant; site 4 (S4): Daqin Village (located 3.6 km northeast of the nearest ISE boundary), site 5 (S5): Mengjiazhuang (located 2.2 km southwest of the nearest ISE boundary). The dominant wind direction surrounding the ISE is greatly controlled by the northeast and southeast wind in winter (our sampling period).

The spatial distribution of the sampling sites is shown in Fig. 1. Road dust samples were collected at five sites (S1–S5). Roof dust samples were collected at S1, S2, S3, and S5, at height of approximately 10 m, 10 m, 10 m, and 15 m above the ground, respectively. The atmospheric particulate matter (PM) samples (A2, A4, A5) were collected at S2, S4, and S5, at heights of approximately 10 m, 13 m, and 15 m above the ground, respectively. Moreover, bare soils were collected at S3. For each type of sample, at least three samples were collected at the same site. Dust particle samples (A1) emitted from the the ISE coking plant were collected at S1.

Road and roof dust samples were collected about 150 g using vacuum cleaners (Samsung, SC88P0). Bare soils were collected up about 500 g to a depth of 20 cm at S3 by shovel. The collected raw road, roof dust, and bare soil samples were air-dried indoors for a period till to the moisture content nearly zero, and then sieved through a 48 mesh sieve (equal to 300 μm) to pretreat the raw dust samples (the screen underflow sample was named laser analysing sample) and then select about 50 g laser analysing sample use 150 mesh sieve (equal to 100 μm) to retreat the samples, and kept the screen underflow for further PAHs analysis (the screen underflow sample was named PAHs analysing sample). Atmospheric PM filter samples ($\text{PM}_{2.5}$ and PM_{10}) were collected at A2, A4, and A5 in winter (December 25–30, 2016). Each quartz filter sample ($\phi 90$ mm) of PM with aerodynamic diameters ≤ 2.5 μm ($\text{PM}_{2.5}$) and aerodynamic diameters ≤ 10 μm (PM_{10}) was collected for 24 h using a median-flow particle sampler (Tianhong, Wuhan, Co. Ltd) with a flow rate of 100 L/min. The dust quartz filter sample (P) from the coking plant chimney at S1 was collected for 20 h to one sample with a flow rate 16.67 L/min by diluting channel sampling equipment (made by Qingdao Laoshan Ltd., Qingdao, China), which was calibrated by a gas mass flow calibrator (API 700, New York, NY, USA).

Serial number	Name	Abbreviations	Number of benzene rings	Limit of detection (µg/mL)	Limit of quantification (µg/mL)
1	Naphthalene	NaP	2	0.002	0.005
2	Acenaphthene	Ace	3	0.004	0.01
3	Acenaphthylene	Acy	3	0.005	0.012
4	Fluorine	Flu	3	0.005	0.013
5	Phenanthrene	Phe	3	0.003	0.008
6	Anthracene	Ant	3	0.004	0.011
7	Fluoranthene	Flua	4	0.007	0.124
8	Pyrene	Pyr	4	0.004	0.013
9	Benzo[a]anthracene	BaA	4	0.002	0.007
10	Chrysene	Chry	4	0.007	0.013
11	Benzo[b]fluoranthene	BbF	5	0.003	0.006
12	Benzo[k]fluoranthene fluoranthene	BkF	5	0.004	0.013
13	Benzo[a]pyrene	BaP	5	0.004	0.007
14	Indeno [1,2,3- <i>cd</i>] pyrene	IcdP	6	0.005	0.015
15	Dibenz[ah]anthracene	DahA	5	0.006	0.013
16	Benzo[ghi]perylene	BghiP	6	0.004	0.013

Table 1. Names and properties of 16 US EPA priority PAHs.

Sample pretreatment and instrumental analysis. Approximately 1.0 g of each PAHs analysing sample (including road, roof dust samples and bare soils) and quartz filter sample (including the atmospheric PM Quartz filter samples and one dust particle sample from the coking plant chimney), were extracted for 16 h at 60 °C with n-hexane, using a set of soxhlet extractors, respectively. The extractant was concentrated to 2–3 mL by a rotary evaporator and then purified through a silica gel column. Then, the eluents were collected and concentrated to 0.5 mL, followed by dilution to 1 mL with n-hexane for the subsequent analysis.

The analysis of PAHs was performed with an electrospray ionization source in single reaction monitoring mode using gas chromatography mass spectrometry with a DB-5MS column (60 m × 0.25 mm × 0.25 µm; Agilent). The instrumental analysis conditions were set as the following: injection temperature of 250 °C, column flow velocity of 1.10 mL/min, split flow ratio of 10:1; column pressure of 69.3 kPa, oven temperature of 40 °C, and sample quantity of 1.0 µL.

The raising temperature program was listed as follows: initial temperature of 70 °C for 1 min; warming to 240 °C at a heating rate of 20 °C/min; and warming to 310 °C at a heating rate of 10 °C/min and maintained for 20 min. The carrier gas was high-purity nitrogen.

The target compounds for monitoring and analysis were 16 types of US EPA PAHs, and the specific substances and their properties, limit of detection, and limit of quantification were shown in Table 1.

Quality control. Among the 16 types of PAHs, only BaA, Chry, IcdP, and DahA of 16 PAHs were detected in the analytical blank samples, whereas others could not be detected within their limit of detection. The detected blank samples average concentration of BaA, Chry, IcdP, and DahA, was 0.0031, 0.0085, 0.0055, and 0.0067 µg/mL, which was very low, indicating that little interference for the target compounds was present in the experiment. These blank samples concentrations were subtracted from the concentrations in the actual samples to account for the blank contamination. The 16 types of PAHs mixed standard solutions (2000 µg/mL, AccuStandard Inc., US) with concentration of 0.2, 0.4, 0.6, 0.8, 1.0, and 2.0 mg/L were configured, with correlation coefficients, R^2 , all above 0.9997. For every ten samples indicator perylene-d12 standard solution (4000 µg/mL, AccuStandard Inc., US) was added to one actual sample and blank sample for the QA/QC, and the recovery efficiency was between 82 and 113% and 78 and 100%, respectively (meeting the EPA requirement 80–120%), and the relative standard deviation (RSD) was 1.74–12.6% and 3.2–11.5%, respectively (meeting the EPA requirement of RSD < 20%).

Particle size analysis method. The laser particle size analyzer (LS-C(I), Zhuhai Omec Company, Zhuhai, China) was used to test the particle size distribution of two typical samples of road dust and roof dust. Before testing the size distribution, the raw dust particle samples were pretreated by 300 µm stainless steel sieve and the pretreated method was listed in 1.1 (laser analyzing sample).

Risk assessment methods. The toxic equivalency value of BaP (TEQ_{BaP}) is used to evaluate the potential ecological risk caused by the PAHs²¹. The calculation method is given in Eq. (1).

$$TEQ_{BaP} = \sum (C_i \times TEF_i), \quad (1)$$

PAHs	S1		S2		S3		S4			S5	
	RD	RF	RD	RF	BS	RD	RF	RD	RD	RF	
NaP	0.730±0.080	0.970±0.092	0.160±0.014	0.080±0.071	0.990±0.088	0.020±0.018	0.070±0.008	N.D	0.060±0.053	0.020±0.002	
Acy	1.610±0.153	0.260±0.025	0.02±0.002	0.010±0.001	0.040±0.004	0.020±0.002	0.010±0.001	N.D	0.010±0.001	N.D	
Ace	0.140±0.093	0.090±0.008	0.02±0.002	0.010±0.001	0.100±0.009	0.010±0.001	0.010±0.001	N.D	0.010±0.001	0.010±0.001	
Flu	0.730±0.069	0.420±0.040	0.09±0.011	0.030±0.027	0.150±0.015	0.010±0.001	0.010±0.001	N.D	0.050±0.005	N.D	
Phe	3.570±0.303	1.700±0.162	0.21±0.019	0.250±0.024	1.070±0.102	0.120±0.012	0.230±0.025	0.020±0.002	0.290±0.028	0.060±0.007	
Ant	1.440±0.130	0.350±0.040	0.040±0.004	0.030±0.004	0.080±0.010	0.040±0.005	0.020±0.002	0.010±0.001	0.050±0.006	0.010±0.001	
Flua	4.620±0.439	1.970±0.213	0.130±0.014	0.360±0.032	1.310±0.144	0.260±0.025	0.470±0.042	0.040±0.004	0.260±0.023	0.060±0.006	
Pyr	3.060±0.127	1.250±0.113	0.120±0.012	0.270±0.020	1.130±0.021	0.160±0.014	0.260±0.029	0.030±0.004	0.330±0.036	0.040±0.005	
BaA	3.350±0.285	0.990±0.089	0.160±0.018	1.730±0.156	0.540±0.049	0.180±0.015	0.430±0.041	0.050±0.005	0.590±0.053	0.080±0.007	
Chry	3.430±0.307	1.820±0.127	0.170±0.015	1.900±0.171	2.710±0.300	0.330±0.031	0.460±0.044	0.050±0.006	0.640±0.061	0.080±0.010	
BbF	7.270±0.118	2.280±0.196	0.070±0.008	0.580±0.055	2.140±0.311	0.360±0.034	0.240±0.023	0.060±0.053	0.290±0.025	0.070±0.008	
BkF	7.270±0.121	2.280±0.196	0.070±0.008	0.580±0.055	1.820±0.164	0.360±0.020	0.240±0.021	0.060±0.005	0.290±0.021	0.070±0.008	
BaP	3.030±0.118	0.880±0.079	0.030±0.003	0.210±0.021	0.630±0.069	0.120±0.013	0.070±0.006	0.040±0.004	0.210±0.019	0.040±0.004	
IcdP	2.730±0.127	0.710±0.067	0.030±0.004	0.160±0.017	0.410±0.044	0.080±0.071	0.050±0.006	0.040±0.004	0.120±0.013	0.050±0.007	
DahA	1.190±0.107	0.280±0.025	0.030±0.003	0.100±0.009	0.170±0.015	0.050±0.044	0.030±0.027	0.030±0.002	0.100±0.013	0.030±0.004	
BghiP	2.800±0.122	0.890±0.080	0.030±0.003	0.260±0.023	0.700±0.067	0.090±0.080	0.060±0.007	0.040±0.004	0.210±0.186	0.050±0.005	
Σ ₁₆ PAHs	46.970±4.791	17.140±4.462	1.370±0.117	6.550±0.583	13.990±1.203	2.210±0.188	2.660±0.246	0.460±0.043	3.510±0.325	0.670±0.062	

Table 2. Concentration of PAHs (µg/g) in the RD, RF, and BS from five sites surrounding the ISE. *N.D.* not detected.

where C_i is the concentration of the i th type of PAHs µg/g, TEF_i is the toxic equivalency factor of the i th type of PAHs (Table 3), and TEQ_{BaP} is the BaP-based toxic equivalency value (µg/g)²².

The carcinogenic risk of PAHs to human health is manifested in three ways: direct ingestion, inhalation, and dermal contact²³. The effect of PAHs on human health is calculated according to the carcinogenic health risk assessment model recommended by the US EPA²⁴. The calculation formulas are listed as follows.

$$ILCR_{ing} = \frac{TEQ_{BaP} \times CSF_{ing} \times \sqrt[3]{BW/70} \times IR_{ing} \times EF \times ED}{BW \times AT \times 10^6}, \quad (2)$$

$$ILCR_{inh} = \frac{TEQ_{BaP} \times CSF_{inh} \times \sqrt[3]{BW/70} \times IR_{inh} \times EF \times ED}{BW \times AT \times PEF}, \quad (3)$$

$$ILCR_{derm} = \frac{TEQ_{BaP} \times CSF_{derm} \times \sqrt[3]{BW/70} \times SA \times SL \times ABS \times EF \times ED}{BW \times AT \times 10^6}, \quad (4)$$

$$TILCR = ILCR_{ing} + ILCR_{inh} + ILCR_{derm}. \quad (5)$$

In Eqs. (2–5), $ILCR_{ing}$, $ILCR_{inh}$, and $ILCR_{derm}$ are the carcinogenic health risk values of ingestion, inhalation, and skin contact, respectively. $TILCR$ is the sum of the three carcinogenic health risks; IR_{ing} is the ingesting rate (mg/day); IR_{inh} is the inhalation rate (m³/day), EF is the exposure frequency (d/a), ED is the exposure duration (a), BW is the body weight (kg), AT is the average exposure time (a), PEF is the particulate matter emission factor (m³/kg); SL is the skin adhesion [mg/(cm² day)], SA is the exposed skin area (cm²), ABS is the skin absorption factor; and CSF_{ing} , CSF_{inh} , and CSF_{derm} are the carcinogenic slope coefficients of the three exposure pathways, which are 7.3, 3.85, and 25.0, respectively (kg d)/mg. When $ILCR$ or $TILCR$ is below 10⁻⁶, between 10⁻⁶ and 10⁻⁴, or above 10⁻⁴, this means that there is no carcinogenic risk, low to moderate carcinogenic risk, or high carcinogenic risk, respectively²⁵.

Results and discussion

16 US EPA priority PAH concentrations in road dust (RD), roof dust (RF), and bare soil (BS) at different sites were shown in Table 2.

Concentration level of PAHs in dusts. *Concentration level of PAHs in road dust.* The total concentration of the 16 PAHs (Σ₁₆ PAHs) in the road dust samples ranged from (0.460±0.043) to (46.970±4.791) µg/g in Table 2, with an average value of (10.892±1.185) µg/g. Among the five sampling sites, the highest Σ₁₆ PAHs value was found at S1, followed by S5 and S3, and the lowest values appeared at S4, upwind of the ISE. The S1 sampling site, located near the coking plant, had the highest PAH concentration level. This phenomenon was consistent with conclusions from previous studies that showed that the sedimentation rate of PAHs near iron and steel works was much greater than that of the other zones²⁶. Moreover, the wind direction can significantly

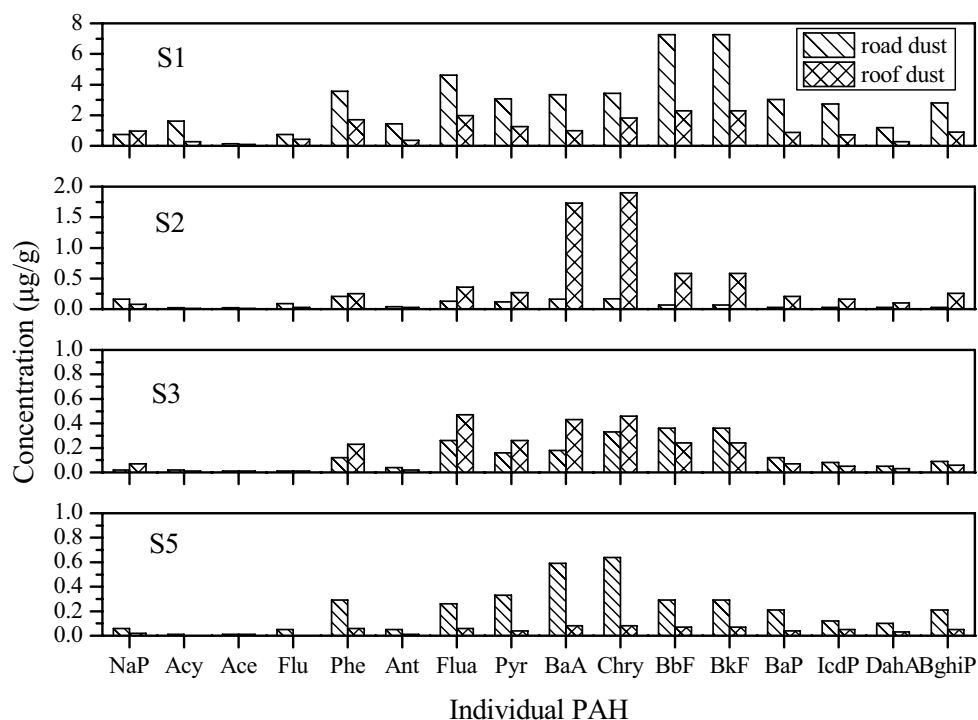


Figure 2. Distribution of PAH of road dust and roof dust at various sampling sites.

affect the PAH concentrations. The Σ_{16} PAHs concentration at S5, downwind of the ISE, was $(3.510 \pm 0.325) \mu\text{g/g}$ and was approximately 7 times the value at S4, upwind of the ISE. In addition, the individual PAH concentrations were all below $0.1 \mu\text{g/g}$, suggesting that it can be affected by wind direction. Vasilakos et al.²⁷ reported that both wind speed and wind direction had an effect on the PAHs concentrations with the source of the pollution coming from different directions.

The most abundant individual PAHs were BbF and BkF in the road dust samples at S1, S3, and S4. However, the dominant compounds were Phe and Chry at S2 and Chry and BaA at S5. Carcinogenic BaP was detected in all dust samples, and the BaP concentration at site S1 near the coking plant had a higher value than that at other sites. Comparison with other reports shows that the average concentrations of PAHs in road dust near the ISE were similar, with a value of $10.62 \mu\text{g/g}$ in Xi'an²⁸, slightly higher than that in Shanghai and Sydney^{29,30}. Notably, in our study area, only the PAHs concentration level at S1 was much higher than previously reported levels, and the concentrations at the other sampling sites were far below those reported in the literature.

Concentration level of PAHs in roof dust. In Table 2, the total concentration of the 16 PAHs was between $(0.670 \pm 0.062) \mu\text{g/g}$ and $(17.140 \pm 4.462) \mu\text{g/g}$ in roof dust, with an average value of $(6.751 \pm 0.692) \mu\text{g/g}$. The highest Σ_{16} PAHs value was found at S1, followed by S2 ($6.550 \pm 0.583 \mu\text{g/g}$) and S3 ($2.660 \pm 0.246 \mu\text{g/g}$), and the lowest values appeared at S5. Because the S1 sampling site was located near the coking plant, the roof dust at this site had the highest PAH concentration. This phenomenon was in accordance with the level of Σ_{16} PAHs in road dust at the S1 site (Table 2). As is known, PAHs are more readily generated during the incomplete combustion of fossil fuels in the coking process, especially in the absence of oxygen³¹. Moreover, the PAH with the highest concentration of roof dust differed at four sites, in which BbF and BkF, Chry, Flua, and BaA and Chry exhibited the highest roof dust concentrations at S1, S2, S3, and S5, respectively. Interestingly, the most abundant PAH for roof dust and road dust at S1 were similar. There is little published data regarding the concentration of PAHs in roof dust; thus, our results are significant in providing some guidance on PAHs pollution.

Distribution of PAHs in dust with sampling height. Road dust and roof dust at the same sample sites were collected from different heights, representing the surface ground (low height) and 10 m height above ground (high height). The distribution of PAHs in dust at different sampling heights was shown in Fig. 2. The PAHs concentrations were higher in roof dust than in road dust at S2 and S3, whereas they were higher in road dust at S1 and S5. The Σ_{16} PAHs level of road dust was almost 2.74 and 5.24 times higher than that of roof dust at S1 and S5, respectively; for example, BbF and BkF at S1 and BaA and Chry at S5 were significantly higher in road dust than in roof dust. Meanwhile, the Σ_{16} PAHs concentration of road dust was 0.21 and 0.82 times lower than that of roof dust at S2 and S3, respectively; for instance, BaA and Chry at S2 were remarkably higher in roof dust than in road dust. This is mainly because the combustion of coal in the coking plant at S1 was a dry distillation process; meanwhile, severe hypoxia and high temperatures in the furnace were conducive to the generation of PAHs. The dust on the roof is not only the receiver of PAHs discharged from the coking plant flue but also the secondary

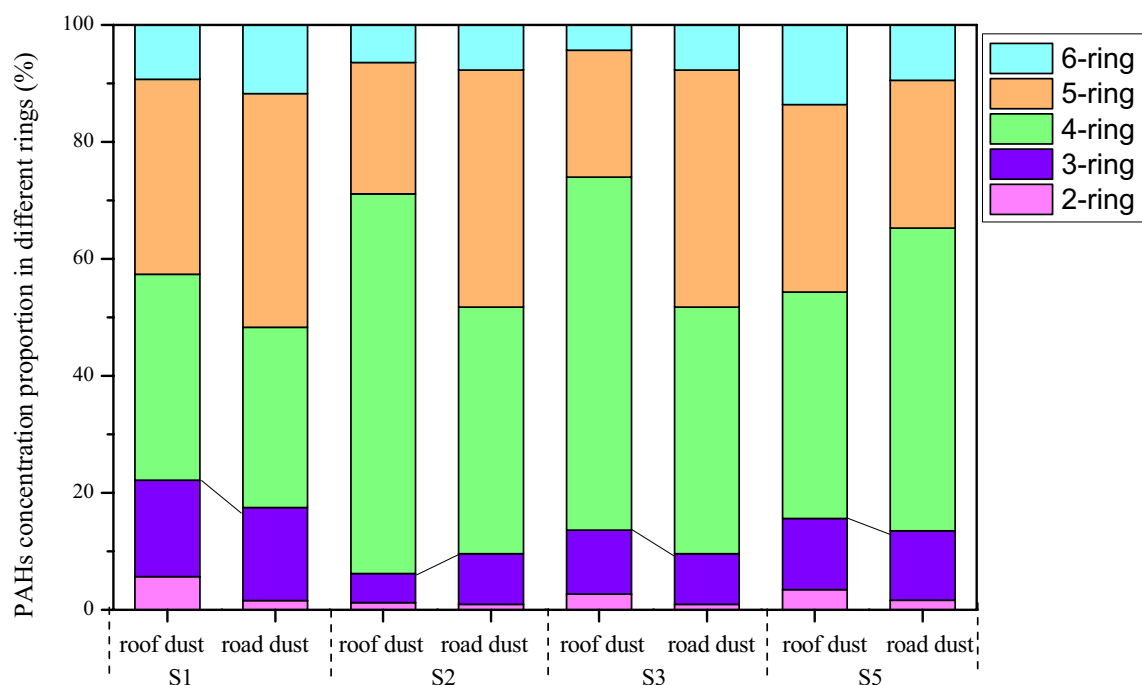


Figure 3. Distribution of PAH with various rings at the sampling sites.

contributors to the road dust. Because of its complex sources, the order of PAH concentrations for the road dust and roof dust was different at the four sampling sites, mainly attributed to the influence of the different sampling sites and the distance to the different industrial processes of the ISE.

PAHs containing four or more rings are defined as high-ring PAHs, whereas others are considered to be low-ring PAHs³². The ring distribution of PAHs in the dust samples are presented in Fig. 3. In this study, different PAH sources, such as road dust and roof dust, have a similar PAH ring distribution such that high-ring PAHs had a higher proportion than low-ring PAHs. Four-ring PAH concentrations were the highest in roof dust at S2 and S3, and road dust at S5, whereas PAHs with four and five rings were both abundant at the other sites, followed by PAHs with three rings. Moreover, high-ring PAHs were mainly present on the surface of the road dust, whereas low-ring PAHs were more likely to exist on roof dust. The abundance of three-to-five-ring PAHs in the dust indicated that the dusts were exposed for a long time to PAHs that originated from industrial activities in these areas.

Typical samples of roof dust and road dust were collected to illustrate their particle size distribution. As were shown in Fig. 4, road dust sample showed a skewed distribution and leaned toward larger particles, whereas roof dust sample exhibited a normal distribution. The peak of the particle size distribution of roof dust and road dust reached 46.13 μm and 80.46 μm , in which the maximum proportion was 8.50% and 8.91%, respectively. D_{10} – D_{90} in road dust (12.42–200.32 μm) was larger than that in roof dust (5.44–149.16 μm), which indicated the compositional complexity of road dust. The D_{50} of road dust (75.30 μm) was higher than that of roof dust (32.63 μm). The particle size of roof dust was finer, whereas the particle size of road dust was coarser.

Concentration level of PAHs in bare soil. The sampling site of bare soil in this study is located in the steelmaking plant (S3). The total concentration of PAHs (Σ_{16} PAHs) was 13.990 ± 1.203 $\mu\text{g/g}$ in bare soil (Table 2). Among these PAHs, Chry had the highest concentration (2.710 ± 0.300 $\mu\text{g/g}$), followed by BbF (2.140 ± 0.311 $\mu\text{g/g}$) and BkF (1.820 ± 0.164 $\mu\text{g/g}$). The concentrations of Acy, Ant, Ace, and Flu were quite lower. Notably, the concentration of BaP, a carcinogenic PAH, was 0.630 ± 0.069 $\mu\text{g/g}$.

Currently, some reports are available concerning the concentration of PAHs in the soil surrounding steelmaking plants in China. Dong et al.³³ found the concentrations of the sixteen PAHs to be between 0.02 and 20.06 $\mu\text{g/g}$ (mean value of 2.56 $\mu\text{g/g}$), among which the BaP concentration was 0.16 $\mu\text{g/g}$ in soil surrounding a steelmaking plant in northern China. However, Tian et al.³⁴ reported a higher concentration of Σ_{16} PAHs and BaP of 32.10 and 0.58 $\mu\text{g/g}$, respectively, at another steelmaking plant located in northeastern China. Furthermore, the total concentration of these PAHs was up to 32.45 $\mu\text{g/g}$ at a coking plant in Beijing³⁵. From these results, we found the concentration of PAHs of bare soil in our study to be near an average level; it was below average around the steelmaking and coking plants in northeastern China and Beijing but above average near the steelmaking plant in northern China.

Chry is one of the carcinogenic PAHs from coal combustion^{36,37}. The Chry concentration was up to 2.710 ± 0.300 $\mu\text{g/g}$ in our study, which was much higher than the previous reports of 1.57 $\mu\text{g/g}$ ³⁸. There is no currently published evaluation standard for soil PAHs in China; thus, the Canadian soil quality benchmark was used to assess soil quality³⁹. The concentration of BaP was 0.630 ± 0.069 $\mu\text{g/g}$ in the collected bare soil, which

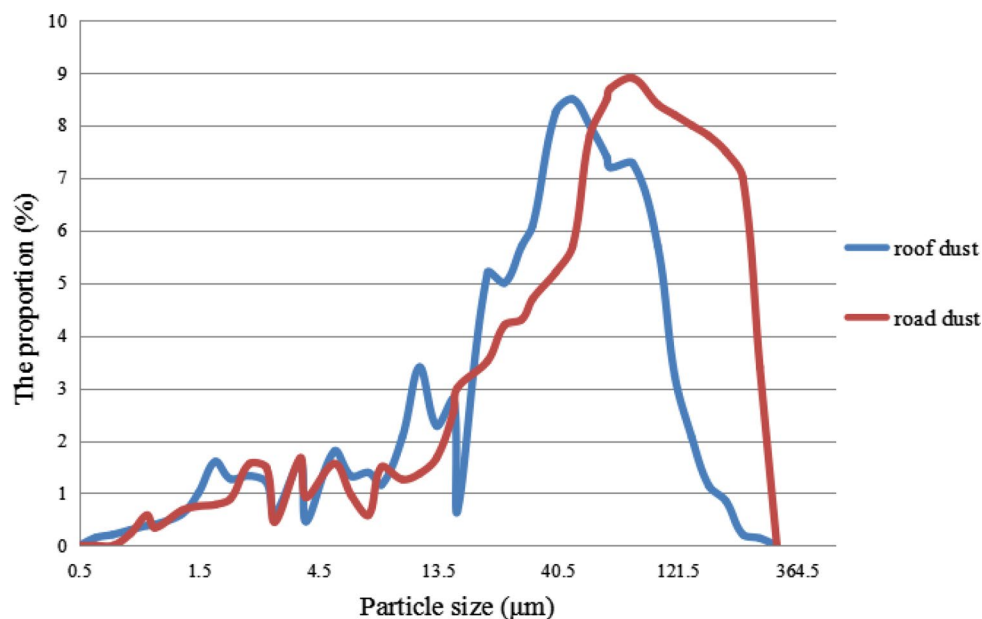


Figure 4. Distribution of particle size in roof dust and road dust.

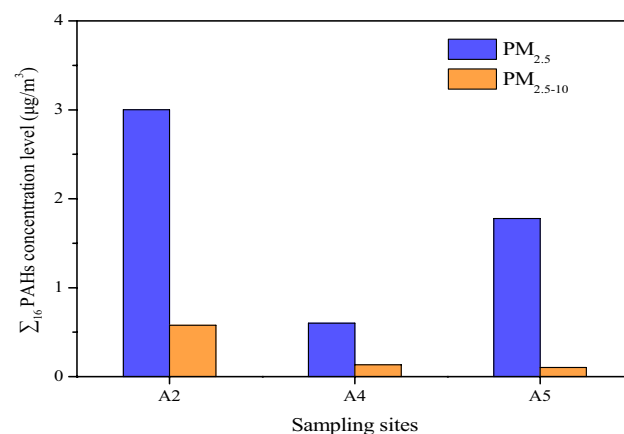


Figure 5. Σ_{16} PAHs concentrations in atmospheric particulate matter (PM), roof dust, and road dust at different sampling sites.

was higher than the reference value of 0.10 $\mu\text{g/g}$ in agricultural soil. Thus, it was indicative of severe pollution in the bare soils in the tested regions.

In summary, different sampling areas contained different PAHs; however, the main types of PAHs in road dust, roof dust, and bare soil at the same sampling site were similar: BbF and BkF were the main pollutants in road and roof dust at S1; BaP and Chry were the main pollutants at S2; the main pollutants were Chry, BbF, and BkF in the bare soil, road dust, and roof dust at S3; the main pollutants were BbF and BkF from road dust at S4; and at S5, the main PAHs were BaP and Chry.

Impact of PAHs in dust on environment atmospheric PM. The Σ_{16} PAHs concentration in $\text{PM}_{2.5}$ and $\text{PM}_{2.5-10}$ at atmospheric PM sites (A2, A4, A5) were shown in Fig. 5. The Σ_{16} PAHs concentration was the highest at A2 inside the iron-smelting plant of the ISE, at 3.01 $\mu\text{g}/\text{m}^3$ in $\text{PM}_{2.5}$ and 0.58 $\mu\text{g}/\text{m}^3$ in $\text{PM}_{2.5-10}$, respectively, and the concentration of Σ_{16} PAHs in A4, upwind of the ISE, was remarkably lower than that in A5, downwind of the ISE. This confirmed that the ISE had a heavy environmental impact on PAHs in the surrounding atmospheric PM, consistent with the research conclusions of related reference⁴⁰. The mass concentration of Σ_{16} PAHs in $\text{PM}_{2.5}$ was 9.741 $\mu\text{g}/\text{m}^3$ in the environmental air, approximately 1 km from a coking plant⁴¹. The Σ_{16} PAHs concentration in our collected samples was lower than that in the literature. The Σ_{16} PAHs concentration proportion of $\text{PM}_{2.5}$ was 81.83% (A2), 83.84% (A4), and 94.49% (A5) of that in PM_{10} . Such a high proportion suggested that PAHs of finer particle size should be given significant emphasis.

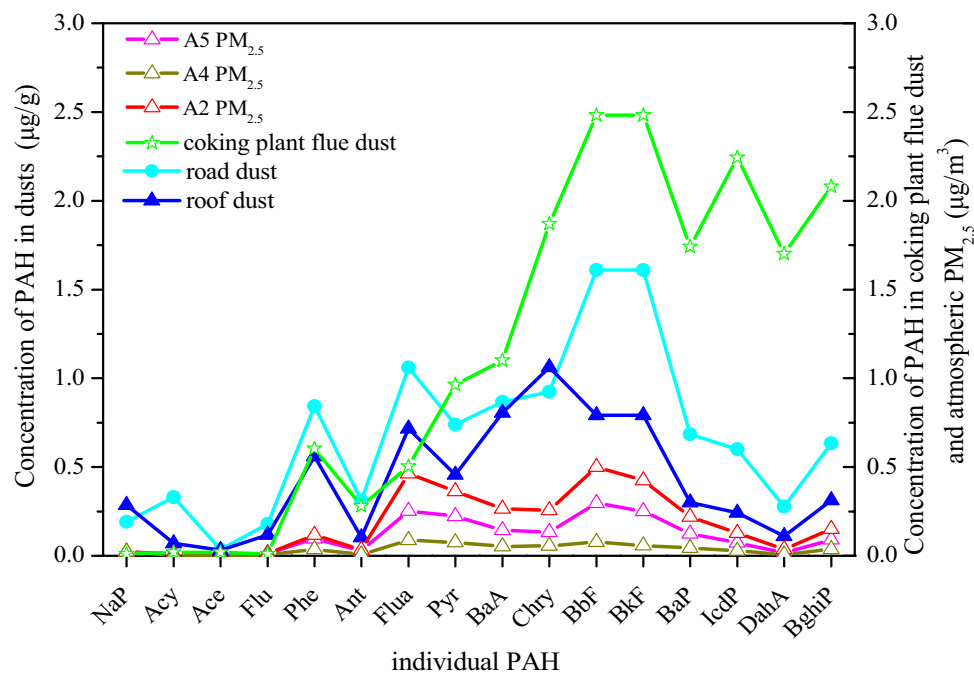


Figure 6. Individual PAH concentrations in dust, coking plant, flue dust, and atmospheric PM_{2.5}.

To reflect the environment impact of individual PAHs from dusts on atmospheric PM, flue dust from one coking plant was collected to compare with the individual PAHs of roof dust and road dust by averaging the data from the different sites. As shown in Fig. 6, road dust and roof dust exhibit similar concentration curves, in which BbF and BkF were the main components of roof dust and road dust, and the PAH with the highest concentration in road dust was Chry. BbF and BkF were also the dominant individual PAHs of the flue dust, whereas the concentration of high-ring PAHs, including BaP, IcdP, DahA, and Behia, was also high. This could be explained as the PAHs with more rings underwent complex physical and chemical reactions in the atmosphere after being discharged from the flue dust, causing a transformation into other environment media. It is reported that high-ring PAHs were derived from the incomplete combustion of fossil fuels and more likely to be adsorbed onto the soil and dust particles^{6,42}. This might also explain the distribution of PAHs in the present study. For atmospheric PM_{2.5}, the concentration curves of the different sample sites were similar; the concentration of BbF was the highest, followed by Flua and BkF. Moreover, the concentration of BaP, a heavily carcinogenic PAH, was 0.50, 0.08, and 0.30 µg/m³ in A2, A4, and A5, respectively, all exceeding the 2nd standard value of the National Ambient Air Quality Standard of BaP (0.0025 µg/m³) in China. Furthermore, BaP/Σ₁₆ PAHs ranged from 7.03 to 9.62% in atmospheric PM_{2.5} and from 4.44 to 6.28% in dusts. Hence, the higher BaP concentration and BaP/Σ₁₆ PAHs value suggested that atmospheric PAHs should be paid much more attention, as they may have a serious impact on the surrounding atmosphere.

Probabilistic health risk assessment of PAHs. The toxic equivalent factors and equivalency values and the carcinogenic risk evaluation results of the 16 PAHs were listed in Table 3. The TEQ_{BaP} values exhibited great differences, depending on the sampling site. For example, the TEQ_{BaP} of the sixteen PAHs was the highest at S1, (1.823 ± 0.091)–(6.370 ± 0.306) µg/g, and it was (0.095 ± 0.008)–(0.638 ± 0.031) µg/g, (0.202 ± 0.017)–(1.330 ± 0.064) µg/g, 0.085 ± 0.004 µg/g, and (0.986 ± 0.009)–(0.443 ± 0.021) µg/g at S2, S3, S4, and S5, respectively (Table 2). The TEQ_{BaP} of the seven carcinogenic PAHs accounted for (93.760 ± 7.969)–(95.590 ± 8.125)% of the total TEQ_{BaP} of 16 PAHs, indicating that these carcinogenic PAHs led to the ecological risk. Among the seven carcinogenic PAHs, the health risk of BaP was the highest. The Σ₁₆TEQ_{BaP} of the various dust samples followed the order: road dust at S1 (6.370 ± 0.306 µg/g) > roof dust at S1 (1.823 ± 0.091 µg/g) > bare soil at S3 (1.330 ± 0.064 µg/g) > roof dust at S2 (0.638 ± 0.031 µg/g) > road dust at S5 (0.443 ± 0.021 µg/g) > road dust at S3 (0.272 ± 0.013 µg/g) > roof dust at S4 (0.202 ± 0.017 µg/g) > roof dust at S5 (0.099 ± 0.009 µg/g) > road dust at S2 (0.096 ± 0.008 µg/g) > road dust at S4 (0.085 ± 0.004 µg/g). Evidently, S1 demonstrated the highest Σ₁₆TEQ_{BaP}. Among the various dust samples, the Σ₁₆TEQ_{BaP} values were higher in road dust than that in roof dust, with the exception of that at S2. There are few reports on the TEQs of PAHs in dust samples. Taking that into consideration, a rough comparison was made regarding the TEQs of PAHs in soils from the different sampling sites in and around an ISE, which showed that the Σ₁₆TEQ_{BaP} and Σ₇TEQ_{BaP} were 0.340 and 0.330 µg/g, respectively, and the Σ₇TEQ_{BaP} to Σ₁₆TEQ_{BaP} ranged from 76.400 to 99.100%⁴³. These findings indicated that carcinogenic PAHs were the main contributors to the total TEQ_{BaP}. Moreover, the concentration of carcinogenic PAHs in our study was higher than that Tao reported in the literature⁴³, suggesting a heavier potential ecological risk for these carcinogenic PAHs in the investigated regions.

PAH	TEF	S1		S2		S3		S4		S5	
		Rd	Rf	Rd	Rf	Bs	Rd	Rf	Rd	Rf	
NaP	0.001	0.728 ± 0.061	0.970 ± 0.077	0.155 ± 0.017	0.080 ± 0.010	0.992 ± 0.011	0.020 ± 0.002	0.070 ± 0.008	N.D.	0.057 ± 0.007	0.020 ± 0.002
Acy	0.001	1.611 ± 0.128	0.260 ± 0.020	0.016 ± 0.001	0.010 ± 0.010	0.043 ± 0.046	0.016 ± 0.002	0.010 ± 0.001	N.D.	0.010 ± 0.001	N.D.
Ace	0.001	0.136 ± 0.010	0.090 ± 0.010	0.023 ± 0.002	0.010 ± 0.197	0.103 ± 0.185	0.006 ± 0.001	0.010 ± 0.001	N.D.	0.012 ± 0.001	0.010 ± 0.001
Flu	0.001	0.731 ± 0.057	0.420 ± 0.033	0.094 ± 0.007	0.030 ± 0.406	0.148 ± 0.082	0.013 ± 0.001	0.010 ± 0.001	N.D.	0.054 ± 0.006	N.D.
Phe	0.001	3.573 ± 0.278	1.700 ± 0.144	0.208 ± 0.016	0.250 ± 0.026	1.073 ± 0.091	0.120 ± 0.014	0.230 ± 0.018	0.024 ± 0.003	0.290 ± 0.025	0.060 ± 0.006
Ant	0.01	14.350 ± 1.119	3.500 ± 0.273	0.380 ± 0.030	0.300 ± 0.026	0.750 ± 0.064	0.350 ± 0.030	0.200 ± 0.017	0.070 ± 0.008	0.510 ± 0.043	0.100 ± 0.010
Flua	0.001	4.618 ± 0.360	1.970 ± 0.167	0.130 ± 0.011	0.360 ± 0.031	1.307 ± 0.111	0.261 ± 0.022	0.470 ± 0.040	0.035 ± 0.004	0.260 ± 0.022	0.060 ± 0.006
Pyr	0.001	3.064 ± 0.238	1.250 ± 0.106	0.115 ± 0.009	0.270 ± 0.023	1.128 ± 0.096	0.158 ± 0.013	0.260 ± 0.022	0.032 ± 0.004	0.326 ± 0.028	0.040 ± 0.004
BaA*	0.1	334,700 ± 24,098	99,000 ± 7,722	16,300 ± 1,271	173,000 ± 13,494	53,460 ± 4,170	18,300 ± 1,427	43,000 ± 3,354	5,100 ± 0.434	59,100 ± 4,610	8,000 ± 0.816
Chry*	0.01	34,330 ± 2,677	18,200 ± 0.873	1,680 ± 0.131	19,000 ± 1,520	27,107 ± 2,006	3,250 ± 0.241	4,600 ± 0.340	0.510 ± 0.043	6,400 ± 0.544	0.800 ± 0.082
BbF*	0.1	727,300 ± 52,365	238,000 ± 17,432	6,500 ± 0.507	58,000 ± 4,524	214,17 ± 16,705	36,200 ± 2,824	24,000 ± 2,864	5,700 ± 0.422	29,200 ± 2,278	7,000 ± 0.595
BkF*	0.1	727,300 ± 53,820	228,000 ± 17,784	6,500 ± 0.533	58,000 ± 4,526	181,515 ± 14,158	36,200 ± 2,823	24,000 ± 1,872	5,700 ± 0.445	29,200 ± 1,119	7,000 ± 0.574
BaP*	1	3026,000 ± 217,872	880,000 ± 63,361	33,000 ± 2,574	210,000 ± 16,382	631,500 ± 46,731	121,000 ± 9,438	70,000 ± 5,460	37,000 ± 2,886	207,000 ± 14,904	40,000 ± 3,120
IcdP*	0.1	272,600 ± 21,262	71,000 ± 4,899	3,300 ± 0.227	16,000 ± 1,248	41,445 ± 3,233	8,300 ± 0.647	5,000 ± 0.425	3,800 ± 0.262	11,900 ± 0.928	5,000 ± 0.370
DahA*	1	1191,000 ± 88,134	280,000 ± 20,162	27,000 ± 2,106	100,000 ± 6,900	169,200 ± 13,198	47,000 ± 3,666	30,000 ± 2,340	27,000 ± 2,106	97,000 ± 7,566	30,000 ± 2,340
BghiP	0.01	28,000 ± 1,932	8,900 ± 0.614	0.340 ± 0.039	2,600 ± 0.299	6,948 ± 0.514	0.870 ± 0.102	0.600 ± 0.069	0.380 ± 0.044	2,130 ± 0.245	0.500 ± 0.058
Σ ₁₆ TEQ _{BaP}	/	6370.041 ± 305.761	1823.260 ± 91.163	95.741 ± 8.329	637.910 ± 30.621	1330.887 ± 63.883	272.06 ± 13.059	202.460 ± 17.209	85.351 ± 4.097	443.449 ± 21.286	98.590 ± 8.577
Σ ₇ TEQ _{BaP}	/	6038.920 ± 271.751	1725.870 ± 82.841	89.770 ± 7.630	601.960 ± 28.894	1258.100 ± 56.615	259.830 ± 12.472	192.070 ± 9.219	80.920 ± 3.884	423.890 ± 20.347	92.560 ± 7.868
Σ ₇ TEQ/Σ ₁₆ TEQ(%)	/	94.800 ± 7.204	94.660 ± 8.235	93.760 ± 7.969	94.360 ± 8.209	94.530 ± 8.035	95.500 ± 8.309	94.870 ± 8.064	94.800 ± 8.248	95.590 ± 8.125	93.880 ± 8.168

Table 3. Health risk caused by PAHs in RD, RF, and BS inside the ISE and in the surrounding environment based on the TEQ_{BaP} (× 10⁻³ µg/g). N.D. stands for none detected; PAHs with * refers to carcinogenic PAHs.

Exposure pathways	Age group	S1		S2		S3		S4		S5	
		Rd	Rf	Rd	Rf	Bs	Rd	Rf	Rd	Rf	
ILCR _{ing}	Child	(8.065 ± 0.061) × 10 ⁻⁶	(2.308 ± 0.103) × 10 ⁻⁶	(1.212 ± 0.227) × 10 ⁻⁷	(8.079 ± 0.598) × 10 ⁻⁷	(1.685 ± 0.203) × 10 ⁻⁶	(3.444 ± 0.149) × 10 ⁻⁷	(2.563 ± 0.149) × 10 ⁻⁷	(1.081 ± 0.193) × 10 ⁻⁷	(5.614 ± 0.429) × 10 ⁻⁷	(1.248 ± 0.119) × 10 ⁻⁷
	Adult (male)	(1.144 ± 0.125) × 10 ⁻⁶	(3.274 ± 0.135) × 10 ⁻⁶	(1.719 ± 0.155) × 10 ⁻⁷	(1.146 ± 0.149) × 10 ⁻⁶	(2.390 ± 0.149) × 10 ⁻⁶	(4.886 ± 0.444) × 10 ⁻⁷	(3.636 ± 0.149) × 10 ⁻⁷	(1.553 ± 0.413) × 10 ⁻⁷	(7.964 ± 0.966) × 10 ⁻⁷	(1.771 ± 0.416) × 10 ⁻⁷
	Adult (female)	(1.170 ± 0.109) × 10 ⁻⁶	(3.349 ± 0.444) × 10 ⁻⁶	(1.759 ± 0.163) × 10 ⁻⁷	(1.172 ± 0.103) × 10 ⁻⁶	(2.445 ± 0.249) × 10 ⁻⁶	(4.998 ± 0.324) × 10 ⁻⁷	(3.719 ± 0.149) × 10 ⁻⁷	(1.568 ± 0.416) × 10 ⁻⁷	(8.146 ± 0.973) × 10 ⁻⁷	(1.811 ± 1.216) × 10 ⁻⁷
ILCR _{inh}	Child	(3.753 ± 0.023) × 10 ⁻¹⁰	(1.074 ± 0.498) × 10 ⁻¹⁰	(5.641 ± 0.438) × 10 ⁻¹¹	(3.758 ± 0.211) × 10 ⁻¹¹	(7.841 ± 0.644) × 10 ⁻¹¹	(1.603 ± 0.144) × 10 ⁻¹¹	(1.193 ± 0.197) × 10 ⁻¹¹	(5.028 ± 0.1) × 10 ⁻¹²	(2.613 ± 0.259) × 10 ⁻¹¹	(5.808 ± 0.318) × 10 ⁻¹¹
	Adult (male)	(1.570 ± 0.149) × 10 ⁻⁹	(4.495 ± 0.416) × 10 ⁻¹⁰	(2.360 ± 0.219) × 10 ⁻¹¹	(1.573 ± 0.149) × 10 ⁻¹⁰	(3.281 ± 0.119) × 10 ⁻¹⁰	(6.707 ± 0.179) × 10 ⁻¹¹	(4.991 ± 0.497) × 10 ⁻¹¹	(2.104 ± 0.149) × 10 ⁻¹¹	(1.093 ± 0.106) × 10 ⁻¹⁰	(2.431 ± 0.201) × 10 ⁻¹²
	Adult (female)	(1.316 ± 0.135) × 10 ⁻¹⁰	(3.767 ± 0.355) × 10 ⁻¹⁰	(1.978 ± 0.187) × 10 ⁻¹¹	(1.318 ± 0.216) × 10 ⁻¹⁰	(2.749 ± 0.222) × 10 ⁻¹⁰	(5.621 ± 0.981) × 10 ⁻¹¹	(4.183 ± 0.416) × 10 ⁻¹¹	(1.763 ± 0.144) × 10 ⁻¹¹	(9.161 ± 0.519) × 10 ⁻¹¹	(2.037 ± 0.106) × 10 ⁻¹¹
ILCR _{derm}	Child	(7.834 ± 0.169) × 10 ⁻⁴	(2.242 ± 0.178) × 10 ⁻⁴	(1.177 ± 0.198) × 10 ⁻⁵	(6.069 ± 0.597) × 10 ⁻⁵	(1.637 ± 0.139) × 10 ⁻⁴	(3.346 ± 0.961) × 10 ⁻⁵	(2.490 ± 0.144) × 10 ⁻⁵	(1.050 ± 0.077) × 10 ⁻⁵	(5.454 ± 0.444) × 10 ⁻⁵	(1.213 ± 0.198) × 10 ⁻⁵
	Adult (male)	(6.061 ± 0.249) × 10 ⁻⁴	(1.735 ± 0.198) × 10 ⁻⁴	(9.109 ± 0.776) × 10 ⁻⁶	(5.478 ± 0.446) × 10 ⁻⁵	(1.266 ± 0.149) × 10 ⁻⁴	(2.588 ± 0.931) × 10 ⁻⁵	(1.926 ± 0.179) × 10 ⁻⁵	(8.120 ± 0.498) × 10 ⁻⁶	(4.219 ± 0.419) × 10 ⁻⁵	(9.380 ± 0.799) × 10 ⁻⁶
	Adult (female)	(5.470 ± 0.498) × 10 ⁻⁴	(1.566 ± 0.149) × 10 ⁻⁴	(8.222 ± 0.597) × 10 ⁻⁶	(7.926 ± 0.497) × 10 ⁻⁵	(1.143 ± 0.138) × 10 ⁻⁴	(2.336 ± 0.138) × 10 ⁻⁵	(1.739 ± 0.149) × 10 ⁻⁵	(7.329 ± 0.619) × 10 ⁻⁶	(3.808 ± 0.315) × 10 ⁻⁵	(8.466 ± 0.777) × 10 ⁻⁶
TILCR	Child	(7.915 ± 0.579) × 10 ⁻⁴	(2.265 ± 0.179) × 10 ⁻⁴	(1.190 ± 0.295) × 10 ⁻⁵	(7.926 ± 0.597) × 10 ⁻⁵	(1.654 ± 0.113) × 10 ⁻⁴	(3.380 ± 0.213) × 10 ⁻⁵	(2.516 ± 0.188) × 10 ⁻⁵	(1.061 ± 0.171) × 10 ⁻⁵	(5.510 ± 0.444) × 10 ⁻⁵	(1.225 ± 0.122) × 10 ⁻⁵
	Adult (male)	(6.175 ± 0.601) × 10 ⁻⁴	(1.767 ± 0.169) × 10 ⁻⁴	(9.281 ± 0.479) × 10 ⁻⁶	(6.184 ± 0.588) × 10 ⁻⁵	(1.290 ± 0.143) × 10 ⁻⁴	(2.637 ± 0.167) × 10 ⁻⁵	(1.963 ± 0.179) × 10 ⁻⁵	(8.274 ± 0.793) × 10 ⁻⁶	(4.299 ± 0.416) × 10 ⁻⁵	(9.557 ± 0.792) × 10 ⁻⁶
	Adult (female)	(5.587 ± 0.512) × 10 ⁻⁴	(1.599 ± 0.167) × 10 ⁻⁴	(8.398 ± 0.761) × 10 ⁻⁶	(5.395 ± 0.497) × 10 ⁻⁵	(1.167 ± 0.112) × 10 ⁻⁴	(2.386 ± 0.149) × 10 ⁻⁵	(1.776 ± 0.159) × 10 ⁻⁵	(7.486 ± 0.649) × 10 ⁻⁶	(3.890 ± 0.349) × 10 ⁻⁵	(8.647 ± 0.798) × 10 ⁻⁶

Table 4. Carcinogenic risk evaluation results of the PAHs in RD, RF, and BS inside the ISE and in the surrounding environment.

Carcinogenic risk evaluation results of the PAHs in road dust, roof dust, and bare soil inside the ISE and in the surrounding environment were listed in Table 4. The ranges of TILCR for children, adult males, and adult females were $(1.061 ± 0.171) × 10^{-5}$ – $(7.915 ± 0.579) × 10^{-4}$, $(8.274 ± 0.793) × 10^{-6}$ – $(6.175 ± 0.601) × 10^{-4}$, and $(7.486 ± 0.649) × 10^{-6}$ – $(5.587 ± 0.512) × 10^{-4}$, respectively. Road dust exhibited heavier carcinogenic risk than roof dust, and the TILCR of bare soil at S3 was higher than that of road dust and roof dust, indicating potentially heavier pollution in bare soil. Among the different exposure pathways, the order of the carcinogenic risk value was $ILCR_{derm} > ILCR_{ing} > ILCR_{inh}$. $ILCR_{inh}$ did not indicate any carcinogenic risk as the value was lower than 10^{-6} . $ILCE_{ing}$ in road and roof dust at S1, roof dust at S2, and bare soil at S2 were between 10^{-6} and 10^{-4} , suggesting a low to moderate risk of carcinogenesis, and LCE_{derm} of road and roof dust at S1 and bare soil at S2 exceeded 10^{-4} , indicating a higher carcinogenesis risk. For different age groups, $ILCR_{ing}$ and $ILCR_{inh}$ in adults were higher than in children, whereas the $ILCR_{derm}$ value for children was slightly higher than that for adults, indicating that the carcinogenesis risk was increasing with age, but children was easily to suffer from skin contact. Moreover, male $ILCR_{inh}$ and $ILCR_{derm}$ was higher than female, while male $ILCR_{ing}$ was lower than that of female, mainly because of the female lower respiratory rate, lower weight, lower skin contact area, and longer lifetime²⁵.

Conclusions

To investigate the concentration levels of 16 priority PAHs in road dust and in roof dust inside and in the surrounding region of the ISE and its impact on atmospheric PM, dust and environment PM samples were collected. The results showed that PAH concentrations displayed great variability in dusts. The Σ₁₆ PAHs concentrations (in dry weight) were between 0.460 and 46.970 µg/g (avg ± sd 10.892 ± 1.185 µg/g) in road dust, between 0.670 and 17.140 µg/g (avg ± sd 6.751 ± 0.692 µg/g) in roof dust, and 13.990 ± 1.203 µg/g in bare soil. Particle size distribution and PAH distribution of dust samples showed that road dust at low height had a coarser particle size

and easily adsorbed high-ring PAHs (PAHs containing four or more rings). For atmospheric PM sites, Σ_{16} PAHs was the highest inside the ISE, followed by sites downwind of the ISE, and the lowest at sites upwind of the ISE. This indicates a greater impact of dust on the atmospheric PM near the ISE. A similar concentration curve was synchronously observed, whereby the most abundant individual PAHs were BbF, Flua, and BkF at atmospheric PM sites and BbF, Chry, and BkF in dusts. BaP/ Σ_{16} PAHs ranged from 7.03 to 9.62% in atmospheric PM and ranged from 4.44 to 6.28% in dusts, suggesting that PAHs of atmospheric PM should be paid sufficient attention as they may have serious impact on the surrounding atmosphere.

Toxicity analysis revealed that PAHs with four rings, including carcinogenic PAHs, were the dominant pollutants in the studied area, and the $\Sigma_7\text{TEQ}_{\text{BaP}}$ to $\Sigma_{16}\text{TEQ}_{\text{BaP}}$ ratio ranged from 76.400 to 99.100%. Based on the carcinogenic health risk assessment model recommended by the US EPA, the calculated results showed that skin contact with PAHs was the greatest health risk, followed by ingestion and inhalation. By comparison, road dust presented a greater carcinogenic risk than roof dust, while bare soil may suffer from heavier pollution. Meanwhile, the PAH carcinogenic risk of adults by skin contact and inhalation was higher than that of a child, and male PAH carcinogenic risk was higher than that of female.

Received: 28 December 2020; Accepted: 18 February 2021

Published online: 24 March 2021

References

1. Tsapakis, M. & Stephanou, E. G. Occurrence of gaseous and particulate polycyclic aromatic hydrocarbons in the urban atmosphere, study of sources and ambient temperature effect on the gas/particle concentration and distribution. *Environ. Pollut.* **133**, 147–156 (2015).
2. Sun, Y. M. *et al.* Distribution pattern, emission characteristics, and environmental impact of polycyclic aromatic hydrocarbons (PAHs) in download ash and dust from iron and steel enterprise. *Molecules* **24**, 20–24 (2019).
3. Filho, C. M. C. *et al.* Uncommon sorption mechanism of aromatic compounds onto poly(vinyl alcohol)/chitosan/maleic anhydride- β -cyclodextrin hydrogels. *Polymers* **12**(877), 1–23 (2020).
4. US EPA, United States Environmental Protection Agency (10.19, 2013). <http://www.epa.gov/>.
5. Cheng, G. E., Qiong, A. N. & Dong, Y. H. Residue and risk assessment of polycyclic aromatic hydrocarbons (PAHs) in soils around a steel mill. *J. Ecol. Rural Environ.* **21**, 66–66 (2005).
6. Shi, B. F. *et al.* Characteristics and sources of polycyclic aromatic hydrocarbons in surface soil from industrial areas of Baise, Guangxi. *China Environ. Sci.* **34**, 2593–2601 (2014).
7. Gilio, A. D. *et al.* An intensive monitoring campaign of PAHs for assessing the impact of a steel plant. *Chemosphere* **168**, 171–182 (2017).
8. He, F. P. *et al.* Polycyclic aromatic hydrocarbons in soils of Beijing and Tianjin region, vertical distribution, correlation with TOC and transport mechanism. *J. Environ. Sci.* **21**, 675–685 (2009).
9. Wang, H. Current situation of prevention and control of key smoke and dust pollution sources in iron and steel industry. *Chin. Soc. For Environ. Sci.* **3**, 50–52 (2014).
10. Takeshi, O. Spatial distribution and exposure risks of ambient chlorinated polycyclic aromatic hydrocarbons in Tokyo Bay area and network approach to source impacts. *Environ. Pollut.* **232**, 267–274 (2018).
11. Sun, P., Basu, I. & Hites, R. A. Temporal trends of polychlorinated biphenyls in precipitation and air at Chicago. *Environ. Sci. Technol.* **40**, 1178–1183 (2006).
12. Chang, K. F. *et al.* Atmospheric polycyclic aromatic hydrocarbons (PAHs) in Asia: A review from 1999 to 2004. *Environ. Pollut.* **142**, 390–396 (2006).
13. Huang, X. F. *et al.* Annual variation of particulate organic compounds in PM_{2.5} in the urban atmosphere of Beijing. *Atmos. Environ.* **40**, 2449–2458 (2006).
14. Lan, W. S. *et al.* Pollution characterization and source identification and apportionment of polycyclic aromatic hydrocarbons (PAHs) in airborne particulates. *Res. Environ. Sci.* **18**, 18–24 (2005).
15. Cetin, B. *et al.* Ambient concentrations and source apportionment of PCBs and trace elements around an industrial area in Izmir, Turkey. *Chemosphere* **69**, 1267–1277 (2007).
16. Odabasi, M. *et al.* Electric arc furnaces for steelmaking: Hot spots for persistent organic pollutants. *Environ. Sci. Technol.* **43**, 5205–5211 (2009).
17. Kwon, H. O. & Choi, S. D. Polycyclic aromatic hydrocarbons (PAHs) in soils from a multi-industrial city, South Korea. *Sci. Total Environ.* **470–471**, 1494–1501 (2014).
18. Yang, H. H. *et al.* Profiles of PAH emission from steel and iron industries. *Chemosphere* **48**, 1061–1074 (2002).
19. Tsai, J. H. *et al.* Chemical constituents in particulate emissions from an integrated iron and steel facility. *J. Hazard Mater.* **147**, 111–119 (2007).
20. Li, Y. X. *et al.* Concentration characteristic and ecological risk assessment of polycyclic aromatic hydrocarbons in the surface soils of a steel plant. *Environ. Chem.* **36**, 1320–1327 (2017).
21. Zhou, W. W. *et al.* Distribution, sources, and ecological risk assessment of polycyclic aromatic hydrocarbons (PAHs) in soils of the central and eastern areas of the Qinghai-Tibetan Plateau. *Environ. Sci.* **39**, 1413–1420 (2018).
22. Agarwal, T. *et al.* Pattern, sources and toxic potential of PAHs in the agricultural soils of Delhi, India. *J. Hazard Mater.* **163**, 1033–1039 (2009).
23. USEPA, United States Environmental Protection Agency. Exposure factors handbook [R]. EPA/600/P-95/002Fa. Washington, DC: USEPA, 4:96–103 (2011).
24. USEPA, United States Environmental Protection Agency. Supplemental guidance for developing soil screening levels for superfund sites[R]. Washington, DC: Office of Emergency and Remedial Response, 3:68–72 (2002).
25. Knafla, A., Phillipps, K. A. & Brecher, R. W. Development of a dermal cancer slope factor for benzopyrene. *Regul. Toxicol. Pharm.* **45**, 159–168 (2006).
26. Amodio, M. *et al.* A monitoring strategy to assess the fugitive emission from a steel plant. *Atmos. Environ.* **79**, 455–461 (2013).
27. Vasilakos, C. *et al.* Gas-particle concentration and characterization of sources of PAHs in the atmosphere of a suburban area in Athens, Greece. *J. Hazard Mater.* **140**, 5–51 (2007).
28. Wei, C. *et al.* Occurrence, gas/particle partitioning and carcinogenic risk of polycyclic aromatic hydrocarbons and their oxygen and nitrogen containing derivatives in Xi'an, central China. *Sci. Total Environ.* **505**, 814–822 (2015).
29. Nguyen, T. C. *et al.* Polycyclic aromatic hydrocarbons in road-deposited sediments, water sediments, and soils in Sydney, Australia: Comparisons of concentration distribution, sources and potential toxicity. *Ecotoxicol. Environ. Saf.* **104**, 339–348 (2014).
30. Jia, J. P. *et al.* Characteristics, identification, and potential risk of polycyclic aromatic hydrocarbons in road dusts and agricultural soils from industrial sites in Shanghai, China. *Environ. Sci. Pollut. Res.* **24**, 605–615 (2017).

31. Liu, G. R. *et al.* Atmospheric emission of PCDD/Fs, PCBs, hexachlorobenzene, and pentachlorobenzene from the coking industry. *Environ. Sci. Technol.* **43**, 9196–9201 (2009).
32. Harvey, R. G. *Polycyclic aromatic hydrocarbons: Chemistry and carcinogenicity* (Cambridge University Press, 1991).
33. Dong, J. *et al.* Pollution characteristics and health risk assessment of polycyclic aromatic hydrocarbons in the surface soils of a large steel enterprise in the north of China. *J. Environ. Sci. China* **37**, 3540–3546 (2016).
34. Tian, J. *et al.* Investigation, evaluation and source analysis of PAHs pollution in large steel mills and surrounding soils. *Environ. Chem.* **32**, 1002–1008 (2013).
35. Feng, L. *et al.* Assessment on health risk of polycyclic aromatic hydrocarbons in airborne PM_{2.5} in Tianjin. *Pract. Prev. Med.* **22**, 1322–1325 (2015).
36. Harrison, R. M., Smith, D. J. T. & Luhana, L. Source apportionment of atmospheric polycyclic aromatic hydrocarbons collected from an urban location in Birmingham, UK. *Environ. Sci. Technol.* **30**, 825–832 (1996).
37. Mastral, A. M., Callén, M. & Murillo, R. Assessment of PAH emissions as a function of coal combustion variables. *Fuel* **75**, 1533–1536 (1996).
38. Hou, Y. W. & Zhang, Y. C. Characteristics and risk analysis of PAHs pollution in surface soil of a steel plant in Fujian province. *Environ. Chem.* **31**, 1542–1548 (2012).
39. Kong, L. L. *et al.* Concentration and origin of polycyclic aromatic hydrocarbons in the soil of Dagang Oil Field. *Environ. Sci. Technol.* **41**, 159–165 (2018).
40. Castro, J. *et al.* Polycyclic aromatic hydrocarbons (PAHs) in the Mediterranean Sea: Atmospheric occurrence, deposition and decoupling with settling fluxes in the water column. *Environ. Pollut.* **166**, 40–47 (2012).
41. Wang, J., Zhu, L. Z. & Shen, X. Y. PAHs pollution in air of coke plant and health risk assessment. *Environ. Sci.* **24**, 135–138 (2003).
42. Duan, Y. H. *et al.* Characteristics of polycyclic aromatic hydrocarbons in agricultural soils at a typical coke production base in Shanxi, China. *Chemosphere* **127**, 64–69 (2015).
43. Tao, S. Y. *et al.* Polycyclic aromatic hydrocarbons pollution region in soils of typical coal-fired pollution region in Shanxi Province. *Eco Sci.* **25**, 2005–2013 (2016).

Acknowledgements

This work was sponsored by the Science and Technology Development Project of Shandong Province (2014GSF117002).

Author contributions

X.W. and Y.S. wrote the main manuscript text and C.D., C.C. and L.Z. prepared figures and Tables. G.Z. checked all the data. All authors reviewed the manuscript.

Competing interests

The authors declare no competing interests.

Additional information

Correspondence and requests for materials should be addressed to Y.S.

Reprints and permissions information is available at www.nature.com/reprints.

Publisher's note Springer Nature remains neutral with regard to jurisdictional claims in published maps and institutional affiliations.



Open Access This article is licensed under a Creative Commons Attribution 4.0 International License, which permits use, sharing, adaptation, distribution and reproduction in any medium or format, as long as you give appropriate credit to the original author(s) and the source, provide a link to the Creative Commons licence, and indicate if changes were made. The images or other third party material in this article are included in the article's Creative Commons licence, unless indicated otherwise in a credit line to the material. If material is not included in the article's Creative Commons licence and your intended use is not permitted by statutory regulation or exceeds the permitted use, you will need to obtain permission directly from the copyright holder. To view a copy of this licence, visit <http://creativecommons.org/licenses/by/4.0/>.

© The Author(s) 2021